Title

Demonstration of Feasibility of X-Ray Free Electron Laser Studies of Dynamics of Nanoparticles in Entangled Polymer Melts

Permalink

https://escholarship.org/uc/item/33f9z5z4

Journal

Scientific Reports, 4(1)

ISSN

2045-2322

Authors

Carnis, Jerome
Cha, Wonsuk
Wingert, James
et al.

Publication Date

2014

DOI

10.1038/srep06017

Peer reviewed

SCIENTIFIC REPORTS

Demonstration of Feasibility of X-Ray Free Electron Laser Studies of Dynamics of Nanoparticles in Entangled Polymer Melts

Jerome Carnis[1], Wonsuk Cha[1], James Wingert[2], Jinback Kang[1], Zhang Jiang[3], Sanghoon Song[4], Marcin Sikorski[4], Aymeric Robert[4], Christian Gutt[5,6,7], San-Wen Chen[2], Yeling Dai[2], Yicong Ma[2], Hongyu Guo[2], Laurence B. Lurio[8], Oleg Shpyrko[2], Suresh Narayanan[3], Mengmeng Cui[9], Irem Kosif[9], Todd Emrick[9], Thomas P. Russell[9], Hae Cheol Lee[10], Chung-Jong Yu[10], Gerhard Grübel[5,6], Sunil K. Sinha[2] & Hyunjung Kim[1]

[1]Department of Physics, Sogang University, Seoul 121-742, Korea, [2]Department of Physics, University of California, San Diego, CA 92093, USA, [3]Advanced Photon Source, Argonne National Laboratory, Argonne, IL 60439, USA, [4]LCLS, SLAC National Accelerator Laboratory, Menlo Park, CA 94025, USA, [5]Deutsches Elektronen-Synchrotron (DESY), Notkestraβe 85, D-22607 Hamburg, Germany, [6]The Hamburg Centre for Ultrafast Imaging, Luruper Chaussee 149, 22761 Hamburg, Germany, [7]Department of Physik, University of Siegen, D-57068 Siegen, Germany, [8]Department of Physics, Northern Illinois University, De Kalb, IL 60115, USA, [9]Polymer Science and Engineering Department, University of Massachusetts, Amherst, MA 01003, USA, [10]Pohang Accelerator Laboratory, Pohang, Gyeongbuk 790-784, Korea.

The recent advent of hard x-ray free electron lasers (XFELs) opens new areas of science due to their exceptional brightness, coherence, and time structure. In principle, such sources enable studies of dynamics of condensed matter systems over times ranging from femtoseconds to seconds. However, the studies of "slow" dynamics in polymeric materials still remain in question due to the characteristics of the XFEL beam and concerns about sample damage. Here we demonstrate the feasibility of measuring the relaxation dynamics of gold nanoparticles suspended in polymer melts using X-ray photon correlation spectroscopy (XPCS), while also monitoring eventual X-ray induced damage. In spite of inherently large pulse-to-pulse intensity and position variations of the XFEL beam, measurements can be realized at slow time scales. The X-ray induced damage and heating are less than initially expected for soft matter materials.

S ince the recent availability of X-ray free electron lasers (XFELs) in the hard x-ray regime, many new scientific areas have been explored due to their unprecedented flux, coherence, and time structures[1–3]. Dynamics of complex materials are one of the important areas to investigate with XFELs[4]. The brilliance of these machines, a billion times higher than that of third generation synchrotrons, allows experiments in ranges where the scattering intensity was too low previously, but concomitantly raises the issue of beam damage and other beam induced effects such as sample heating. The fully transversely coherent beam constitutes an unexcelled asset compared to the third generation synchrotron sources, but the random nature of the SASE emission process[5] of XFEL radiation implies pulse-to-pulse variations of the longitudinal coherence length[6] and intensity. It therefore induces contrast variations and sets an upper limit on the accessible wave vector transfer range for experiments relying on the spatial coherence of the beam[7]. The coherence characteristics of the beam were verified from detailed photon statistics analysis[5,8–10].

There are three different possible experimental regimes of XFEL studies related to the photon density at the sample: (i) extremely high photon flux in a small beam size, i.e. in the regime of "diffract before destroy", where the sample is irreversibly damaged after a single pulse and ultrafast X-ray induced electronic processes are investigated; (ii) medium photon fluxes and beam sizes, where the sample can endure a few pulses at least, and damage is on a spatial scale that does not impede the intended experiments. In this case, double shot experiments allow us to study the basic mechanism of X-ray excited phonon states and heat transfer; (iii) low photon densities, where degradation effects of a single pulse can be neglected, sample heating is minimal and
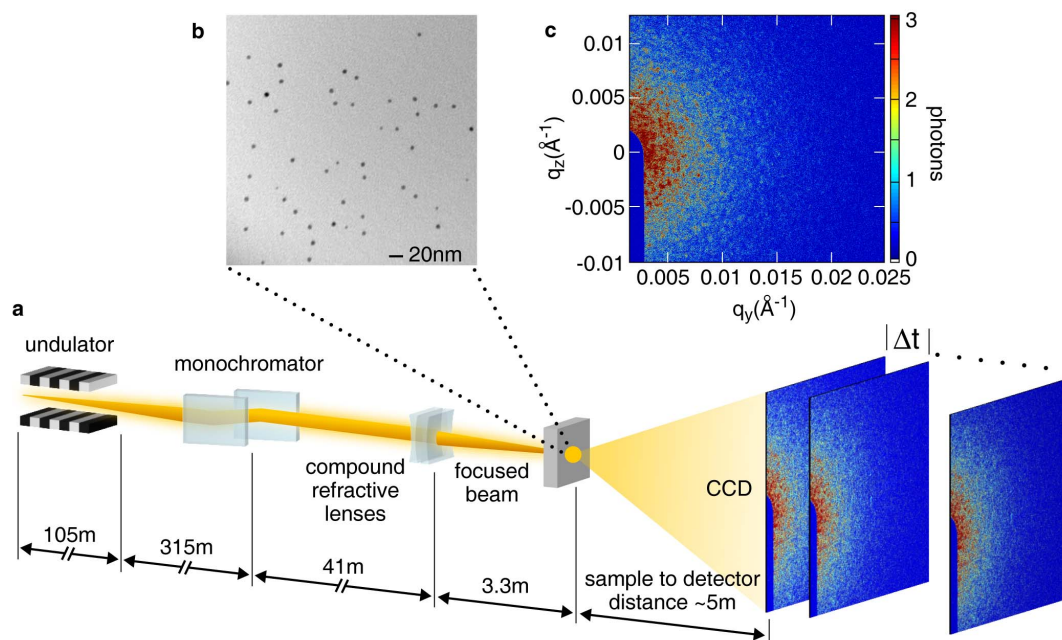
Figure 1 | LCLS XCS experimental setup and measured speckle pattern. (a). XCS instrument experimental setup at LCLS. Successive speckle patterns are recorded with a delay Δt between each frame. (b). TEM image of the gold nanoparticles (5.5 nm dia. nanospheres) grafted polystyrene sample (M_w=42 kg/mol polystyrene matrix). (c). Speckle pattern produced by the fully transverse coherent X-ray beam incident on the sample in (b) in transmission geometry. This pattern was measured at SDD of 5037 mm and at 393 K. The color bar on the right indicates the intensity in the 2D detector converted into photons. The dark blue feature on the left lower part of the image is the beam stop used to mask the direct beam.

multi-pulse exposures are used for equilibrium studies. The boundaries between these regimes obviously depend on the photon flux and sample composition and need to be experimentally determined and verified.

X-ray photon correlation spectroscopy (XPCS) is a powerful technique for probing various steady state [i.e. equilibrium] and non-equilibrium dynamics in condensed matter physics, e.g., the kinetics of de-mixing in crystalline metal alloys[11], magnetic domain switching[12], and polymer relaxation dynamics[13–15]. XPCS typically measures the temporal correlations in the intensity of speckle patterns scattered by disordered systems when illuminated by coherent x-rays with sequential exposures. The feasibility of XPCS with the XFELs was suggested in terms of experimental setup and possible scientific applications involving different temporal regimes[4,16]. For example, a new technical approach with split-and-delay lines[8,17–18] was proposed for probing time scales from femtoseconds to nanoseconds by splitting the beam, delaying one, and collinearly recombining the essentially identical beams with a tuned delay before impinging them on the sample. Other approaches in data analysis, e.g., speckle visibility analysis[19–21] are also being developed to get to time scales faster than those available from sequential XPCS. Prior to the current experiment, sequential XPCS had not yet been realized with the XFEL because of the complications of large pulse-to-pulse intensity variations and the potential X-ray induced sample damages.

In terms of the damage issue, the thresholds for disturbing the atomic arrangements by a single XFEL pulse were for example studied recently in a Ni_2Pd_2P glass[10]. It is of primary importance, though, to take into account multiple pulses for low scattering systems. The sample damage from sequential XFEL pulses is a key to interpreting XPCS results, since XPCS requires the recording of hundreds of frames, with one or multiple pulses for each frame.

In this study, we show that one can extract the dynamics of gold nanoparticles in entangled polymer melts using sequential XPCS over time scales for 10 to 10^3 seconds despite the large intrinsic fluctuations of the XFEL beam. We demonstrate that an experimental window exists for soft-matter materials to study steady state

fluctuation dynamics before X-ray induced damage is of concern. A two-time correlation method was applied to analyze the results obtained by sequential XPCS. Adiabatic heating and steady-state heating on the sample were also estimated for quantifying beam induced effects. These XPCS experiments show that the amount of heat deposited is highly overestimated by the simple energy deposition formula and suggest that more complex heat diffusion processes are in play.

Results

The experiment was performed at the X-ray Correlation Spectroscopy (XCS) instrument[22] at the Linac Coherent Light Source (LCLS) at the SLAC National Accelerator Laboratory (Menlo Park, USA). The schematic of the XCS instrument is shown in Fig. 1(a). Figure 1(b) shows a TEM image of the gold nanoparticles in the polymer matrix with the typical sizes and concentrations used in this study, confirming that the gold nanoparticles are not aggregated but well dispersed in the polymer matrix. Figure 1(c) presents a speckle pattern at a sample to detector distance (SDD) of 5037 mm from gold nanospheres of 5.5 nm diameter with polystyrene (M_w=30 kg/mol) attached to the surface in a polystyrene matrix (M_w=42 kg/mol) at the temperature of 393 K. After reaching the equilibrium temperature, a fresh spot on the sample is illuminated for a total of 150 frames with 100 pulses per frame and then the sample position is shifted to an unexposed area. For each frame, 100 pulses were delivered to the sample. In the high intensity zone, at $q \sim 0.0032 Å^{-1}$, an average of 5.95 photons per pixel was measured, whereas at $q \sim 0.024 Å^{-1}$ it drops to only 0.041 photons per pixel.

With a beam size of 4.7 μm × 3.3 μm (H × V), as obtained by knife edge scans, the speckle size in this configuration is estimated to be 153 μm × 218 μm, extending approximately to 8 × 11 pixels on the detector. The average beam size can be obtained by a spatial intensity autocorrelation analysis of the speckle patterns. The detailed process is described in the Supplementary Information. A square area consisting of 50 × 50 pixels centered at $q=0.0038 Å^{-1}$ is shown in Fig. S1(a) and speckles details shown in S1(b). The corres-
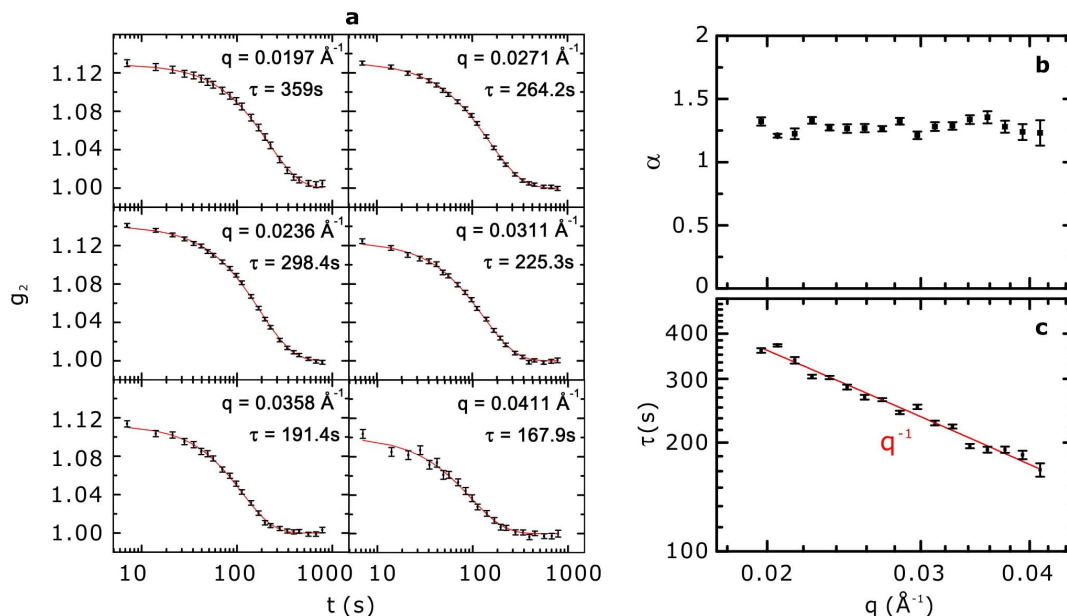
Figure 2 | g₂ functions and relaxation times measured at different wave vector transfers. (a). g_2 functions at different wave vector transfer measured from the same sample. A total of 150 frames with 100 pulses per frame were recorded at each sample position. The red lines are compressed exponential fits to the experimental data. The obtained relaxation time constants are indicated for each plot. (b). Compressed exponent α obtained from the best fit to the g_2 functions. (c). Corresponding q-dependence of the relaxation time constants (τ). The red line is $\tau = q^{-1}$ for comparison.

ponding correlation coefficients calculated from spatial cross-correlations are shown in S1(c). Horizontal and vertical line cuts through the maximum in S1(c) yield the curves plotted in S1(d). Therefore, the average beam size obtained from 100 pulses per frame is 3.5 μm × 3.5 μm (H × V).

Since the speckle pattern is directly related to the positions of the scatters in the sample, a calculation of the correlation between consecutive speckle images allows monitoring the evolution of these positions. As demonstrated in sequential XPCS, at thermal equilibrium, one can follow the polymer relaxation dynamics by registering the evolution of the speckle pattern with time. An important point is to choose a delay time between each frame that is commensurate with the relaxation time to be studied. With the current repetition rate of LCLS, 120 Hz, 8.3 ms sets the lower limit of the relaxation time that can be studied by sequential XPCS. However, in our experiments there is an additional delay of a few seconds arising from the synchronization of the detector and each XFEL pulse, i.e. the read-out time of the detector. Consequently, only the "slow" α relaxation of the polymer chains could be investigated. Independently, insights into X-ray induced damage to the sample could be obtained. At LCLS, each pulse is recorded with its intensity. The data was therefore normalized (see Methods section) by the incident intensity.

The evolution of the speckle patterns are quantified via intensity-intensity correlation functions

$$g_2(\boldsymbol{q},t') = \frac{\langle I(\boldsymbol{q},t)I(\boldsymbol{q},t+t')\rangle_t}{\langle I(\boldsymbol{q},t)\rangle_t^2} = 1 + \beta |f(\boldsymbol{q},t')|^2, \qquad (1)$$

where $f(\boldsymbol{q},t')$ is the intermediate scattering function, β is the speckle contrast, $I(\boldsymbol{q},t)$ is the intensity at wavevector $\boldsymbol{q}$ and time t and $\langle\rangle_t$ represents the time average. The experimental correlation functions are modeled with a stretched exponential using

$$f(\boldsymbol{q},t) = e^{-(t(q)/\tau(q))^{\alpha(q)}}. \qquad (2)$$

The best fits to our data (see Fig. 2a for selected $\boldsymbol{q}$) were obtained using a stretched exponential and $\tau(q)$, the characteristic relaxation time, was allowed to vary as a function of $\boldsymbol{q}$. The red lines are the best

fits to the data, corresponding to an average value of the stretched exponent $\langle\alpha(q)\rangle \sim 1.28$ (i.e. compressed exponential function), shown as a function of wave vector transfer in Fig. 2(b). The characteristic relaxation time scales linearly with the inverse of the wave vector transfer q as shown in Fig. 2(c), where the red line indicates $\tau \sim q^{-1}$.

Contrast obtained from XPCS analysis, $g_2(0)-1$, is compared with the contrast $\beta = 1/M$, where M is the number of modes in the negative binomial distribution,

$$P(I) = \frac{\Gamma(I+M)}{\Gamma(I+1)\Gamma(M)} \left(1 + \frac{M}{<I>}\right)^{-I} (1 + \frac{<I>}{M})^{-M}. \qquad (3)$$

The intensity distributions are obtained in an iso-q annulus centered at q = 0.0032 Å^{-1} with a width of 0.0002 Å^{-1}. $M \sim 12$ was obtained from Fig. S2 and the average of $1/M$ is in agreement with $(g_2(0)-1) \sim 0.08-0.12$ in Fig. 2(a) and Fig. 3(a). More detailed information about the gamma distribution validity[5] can be found in the Supporting Information.

A time evolution of the mechanical and dynamical properties of polymeric materials is often observed when not thermally equilibrated. In our experiments the correlation functions depend not only on the delay time but also on the time the sample was at a specific temperature. As the system evolves towards equilibrium, a slowing-down of the dynamics is generally observed. The $\tau \sim q^{-1}$ dependence with $\alpha \geq 1$ in relaxation time indicates that internal stress relaxation occurs in our samples, which has been observed previously in many systems undergoing aging[23-24] and also in the relaxation time of gold nanoparticle in entangled polymer films[25]. This will be reported in a separate manuscript. Even though the results shown here indicate that sequential XPCS experiments are possible with an XFEL, the X-ray induced damage effects are of concern and must be distinguished from the relaxation of the sample.

We therefore compared the g_2 functions calculated from the first 75 and the last 75 frames of the total of 150 frames collected per measurement. The acquisition time for 75 frames is ~8.5 minutes, corresponding to a total X-ray exposure of ~0.38 ns (estimated using 51 fs pulse duration). Figure 3 shows the changes in the
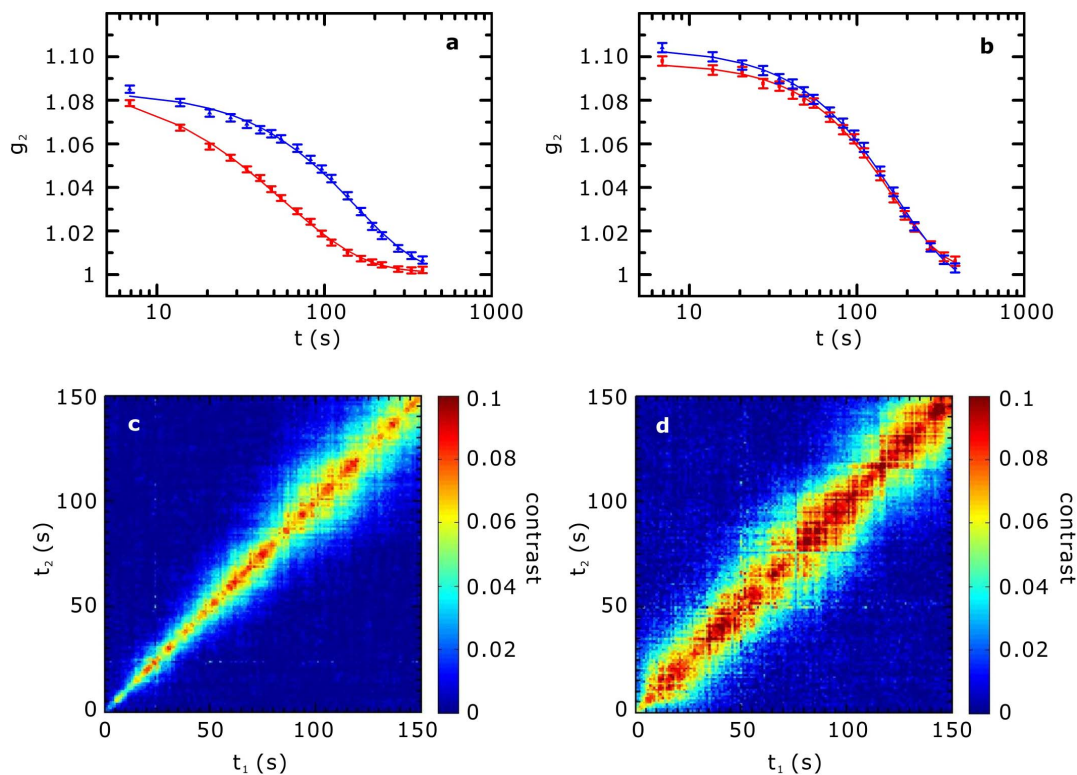
Figure 3 | Evolution of the dynamics at two different ages for a given wave vector transfer. (a). Intensity-intensity autocorrelation function at q=0.0247Å^{-1} at 103 minutes and (b). 477 minutes after the sample reached the temperature of 393 K. g_2 functions are calculated from the first 75 frames (in red) and from the last 75 frames (in blue) among a total 150 frames. (c). Two-time correlations are calculated at the same q for the dataset in (a). (d). those for the data set in (b). The broadening is flagrant in c, whereas the relaxation time is more uniform along the sample age in (d).

dynamics measured 103 and 477 minutes after the sample was thermally equilibrated at 393 K. The g_2 functions shown in red were calculated with first 75 frames and those in blue with the last 75 frames, at $q=0.0247$Å^{-1}. After 103 min. (Fig. 3(a)), the g_2 functions in red show much shorter decay time than those in blue, whereas in (b), the curves in red and in blue are indistinguishable. Further g_2 functions and the corresponding decay time constants at various wave vector transfers are shown in Figure S4 and Table S2, respectively. As indicated in (b), any indication of radiation damage to the sample cannot be discerned from g_2 functions. Consequently, the changes in the relaxation times observed in (a) must be due to the aging of the sample and are not connected to sample damage.

To investigate these changes more in details, the two-time correlation functions[26] can be used to display the time evolution of the dynamics. The two-time intensity correlation function is calculated as

$$C(\boldsymbol{q},t_1,t_2) = \frac{\langle I(\boldsymbol{q},t_1)I(\boldsymbol{q},t_2)\rangle_t - \langle I(\boldsymbol{q},t_1)\rangle_t \langle I(\boldsymbol{q},t_2)\rangle_t}{\sqrt{\langle I^2(\boldsymbol{q},t_1)\rangle_t - \langle I(\boldsymbol{q},t_1)\rangle_t^2}\sqrt{\langle I^2(\boldsymbol{q},t_2)\rangle_t - \langle I(\boldsymbol{q},t_2)\rangle_t^2}}. \quad (4)$$

Typical signatures of aging mechanisms in the two-time correlation can be better understood by the following variables: $\delta t = |t_2 - t_1|$ and $\langle t \rangle = (t_1 + t_2)/2$, where δt represents the distance (in units of time) from the diagonal $t_1 = t_2$, and a constant $<t>$ corresponds to a line perpendicular to the diagonal. We define δt_c as the critical time delay where the contrast is half of its maximum value. If the sample dynamics do not evolve in time, δt_c is constant throughout all the measurements and a straight diagonal line on the plot should be observed. For an aging system, the dynamics slows with time, meaning that the correlations between frames extends to a longer time delay δt, resulting in an increase of δt_c and a broadening in the correlation plot at large $<t>$[26–27]. The results of two-time correlation are shown in Fig. 3(c) and (d) for the same data set in (a) and (b),

respectively. The color bar indicates the contrast for comparison. In (c) the broadening at large time indicates that the sample dynamics is indeed rapidly slowing down, whereas in (d) δt_c remains almost constant even though the value of δt_c is larger than that in (c). Variation of the contrast amplitude on the diagonal itself might be understood as an indirect effect of the shot to shot intensity fluctuations, which cannot be completely removed by normalization.

Figure 4 shows the evolution of $\tau (q)$ for the same sample as in Figs. 2 and 3. For all measurements the SDD was 5037 mm except for the one at 1888 minutes with an SDD=685 mm. In Fig. 4(a), $\tau(q)$s are calculated from the images taken with 1, 2, 10, 30, and 100 pulses per frame successively, for a total of 150 frames, i.e., every 15 to 30 minutes to assess sample damage with a different number of pulses. The sample position was changed after each sequence of 150 frames. In order to see the clear behavior of τ as a function of the time after the sample reached the temperature of 393 K, τ for a single q=0.0123 Å^{-1} is plotted in Fig. 4(b) for the same data set as in (a). There is clearly a trend of slowing down as a function of the number of pulses in the series. It is also obvious that an equilibrium is reached. One has however to keep in mind that each series for a given number of shots per frame, was taken sequentially, thus resulting in measuring the dynamics in the sample at a different age. The observed behavior is more compatible with a "standard aging" behavior than sample heating. For sample heating, one would expect the relaxation time to decrease (i.e. the dynamics to get faster) when more X-rays impinge the sample. Also the aging rate is compatible with what has been observed (cf. Figure 4c), where the typical relaxation time strongly varies over the first 120 minutes and then slows down dramatically for the next 300 minutes).

A significant improvement in the signal to noise ratio is obtained when using more than 10 pulses per frame. In Fig. 4(c), τ (q)s with only 100 pulses per frame are shown at 103, 232, 477, and 1888 min. after reaching the temperature of 393 K where the approach of the
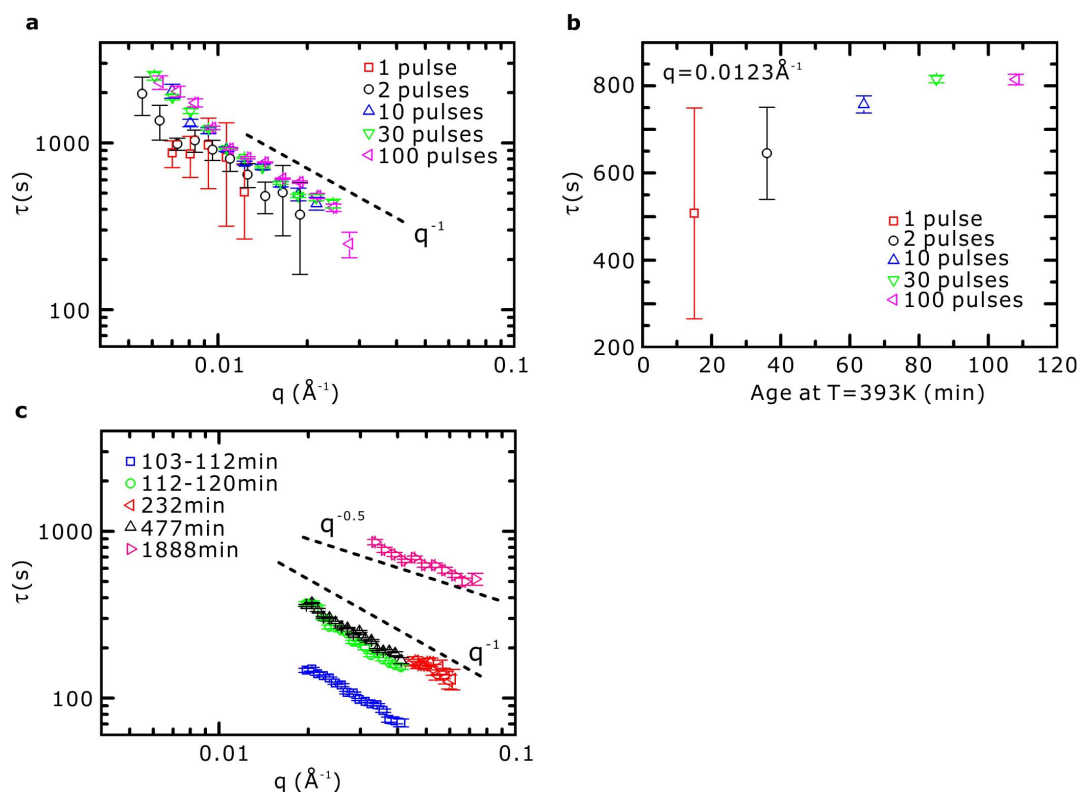
Figure 4 | Evolution of the relaxation time as a function the wave vector transfer. (a). $\tau(q)$ obtained from the images with 1, 2, 10, 30, and 100 pulses per frame measured successively for a total 150 frames. (b). τ at q=0.0123 Å^{-1} as a function of the the age at 393 K for the same data set in (a). (c). Plot of $\tau(q)$ with 100 pulses per frame but at different ages. Position on the sample was changed after each measurement. In (a), the $\tau(q)$s get slower even with increasing number of pulses per frame, as emphasized in (b) for a particular q. In c, the waiting time between the measurements was longer than in (a) to see more clearly the effect of aging. The data for 232 min. was collected at higher q and the error bars are larger than other sets due to lower scattering intensity at high q.

sample to equilibrium is more clearly seen. The data at 103 min. shown in Fig. 3(a) are displayed with the first half (103–112.5 min.) and the last half (112.5–120 min.) frames since the sample is still aging. Since the data at 232 min. was collected for higher q than the other data sets, the errors are larger due to the reduction in the scattering at higher q. All results for less than 477 min. ($\sim$8 hrs) show the $\tau \sim q^{-1}$ dependence, indicating that we are still monitoring quasi-equilibrium fluctuations. By fixing the temperature at 393 K for 1888 min. ($\sim$30 hrs) we found $\tau \sim q^{-0.5}$, which may arise from a more complex long-time relaxation process of the gold nanoparticles. Such scaling was reported for a colloidal gel of adhesive particles[28] and attributed to a probabilistic break-up of aggregates due to weak surface potential interactions. However, in this study, since polystyrene (M_w=30 kg/mol) ligands were anchored to the surface of the gold nanoparticles to prevent aggregation, another mechanism must be invoked.

Since XFEL radiation presents a very different time structure in comparison to synchrotrons, an estimation of beam induced effects needs to be made. Synchrotron sources can be regarded as continuous due to the combination of pulses with picosecond pulse duration and a large repetition rate of several MHz. In contrast, each XFEL pulse has a pulse duration below 100fs (51fs in our case) and a repetition rate of the order of tens of Hz. Consequently, the discontinuous time structure in the XFEL gives a minimum measurable correlation time of a few milliseconds. The high brilliance of such sources raises the possibility of damage after a single pulse; however, the presented results show that it is still possible to study polymeric systems in a sequential manner with no clear observation of damage.

Beam induced sample heating also needs to be taken into account for XFEL experiments where the same location on the sample is

irradiated several times, since the temperature-dependent dynamics would then be different depending on the exposure history. Two origins for sample heating[4,10,16] are considered in the following: (i) adiabatic heating by each single shot and (ii) the steady state heating power due to the exposure of multiple pulses for enhancing the scattering intensity. The average absorbed energy per atom in the illuminated volume is estimated along the lines of the calculations previously published[10].

We calculate the number of photons incident on the sample position by multiplying the transmission coefficients of all the optical components (transmission coefficients can be found in Table S3 in the Supplementary Information). This yields the maximum intensity of $\sim$2.4 $\times$ 10^9 photons per pulse incident on the sample, corresponding to an incoming energy of $\sim$27 J·cm^{-2} for a beam size of 3.5 μm $\times$ 3.5 μm (H $\times$ V) as deduced from speckle size calculation (see Supplementary Information). If this energy is totally transferred to a bulk polystyrene sample, the average absorbed energy per atom in the illuminated volume can be estimated along the lines of the calculation shown in Ref. 10. Since the attenuation length of polystyrene at 8.7 keV ($\sim$2900 μm) is larger than the sample thickness $\sim$ 1 mm we use the latter for the calculation. We obtain an average of 4.8 $\times$ 10^{-3} eV per atom for polystyrene. Using a typical heat capacity of $3k_B$=2.6 $\times$ 10^{-4} eV·K^{-1}, this yields an adiabatic temperature increase of $\sim$18 K per atom for polystyrene. We consider now the energy absorbed by an isolated gold nanoparticle. A simple calculation using gold absorption cross-section and the known experimental parameters yields an average of $\sim$5.41 photons absorbed per nanosphere, corresponding to 9.15 eV per gold atom (see Supplementary information for details). If all the energy were to stay in the nanoparticle, this would lead to an increase of its temperature

by 3.5×10^4 K, where we used the gold specific heat $C_v = 129.1$ J.kg^{-1}.K^{-1}. With such heating the gold nanoparticles would literally explode and this should appear in the correlation functions. The fact that up to 150 frames yield smooth g_2 functions indicates that there exist other mechanisms allowing the absorbed energy to leave the gold nanospheres. The key point is to be attributed to the small size of the nanoparticles.

One can get a qualitative idea regarding the ongoing process by considering the inelastic mean free path of first and secondary electrons generated by the X-ray irradiation: since the X-ray energy (8.7 keV) is lower than the binding energy of the K- and L-shells of gold electrons[29], X-rays ionize gold atoms by expelling mainly M shell electrons, while higher subshell electrons contribute very little to the photoelectric absorption due to their reduced cross section[30]. The difference between the X-ray photon energy and binding energies of M shell electrons ($2 \sim 3$ keV) corresponds to a residual kinetic energy of ~5 to 6 keV. The electron inelastic mean free path in gold at such energies is of the order of 5 to 6 nm[31]. This means that these primary electrons can escape the gold nanoparticle (5.5 nm diameter) and may lose energy in the polymer matrix. Ionized gold atoms may then decay to a lower energy state by the emission of a photon[32] (e.g. $M_{\alpha 1}$ fluorescence emission line at ~2123 eV) or an Auger electron[33] (main peaks at 2024 and 2111 eV). However, the average M shell fluorescence yield is of the order of $2.7 \sim 2.9\%$[34]. Therefore the majority of decays occur through non-radiative processes. The electron inelastic mean free path in gold corresponding to the main peaks of the Auger electrons is ~2.2 nm, close to the radius of the nanospheres, meaning that a non-negligible part of secondary electrons will also escape the nanoparticles and lose energy in the polystyrene matrix.

The steady-state thermal heating power needs only to be considered when multiple pulses are sent to the sample. During the exposure with multiple shots the sample is heated if the time constant for viscous flow τ_{vf} is much smaller than the time constant for thermal diffusion τ_{th}, meaning that the sample literally melts because of the heat load. The time constant for viscous flow can be calculated[10] as $\tau_{vf} = 6\eta(1-v)/E$, where η is the viscosity, v is the Poisson's ratio, and E is the Young's modulus. Since the gold nanoparticles are of very low density (i.e., 0.5% volume fraction), we use $\eta \sim 1 \times 10^8$ N·s·m^{-2}, $v =$ 0.325, and $E = 3.2 \sim 3.4 \times 10^9$ N·m^{-2}, tabulated values for $M_w = 42$ kg/mol polystyrene[35-36] at 393 K and we obtain $\tau_{vf} \approx 10^{-1}$ s. The time constant for thermal diffusion can be estimated[10] from the thermal diffusivity of bulk polystyrene $D_{th} \sim 9.9 \times 10^{-8}$ m^{2}s^{-1} at 393 K: $\tau_{th} = r^2/4D_{th}$, using a length scale of 5 microns for r (approximately the beam size), we obtain $\tau_{th} \approx 6.3 \times 10^{-5}$ s. Since the thermal diffusivity of gold is orders of magnitude greater than polystyrene (D_{th}(Au) $\sim 1.27 \times 10^{-4}$ m^2/s), our simple estimation yields an upper limit for τ_{th}. This indicates that our sample system is far from the regime of strong damage in the 120 Hz repetition rate (8.3 ms between each pulse). This result also confirms that scattering experiments with soft matter at an XFEL are feasible.

Another concern raised by the possibility of measurement at high wave vector transfers is the reduction of the contrast when the path length difference of photons in the sample is close to or larger than the longitudinal coherence length, Λ, defined by $\Lambda = \lambda^2/2\Delta\lambda$, where λ is the wavelength of the radiation. The longitudinal coherence length is inversely proportional to the monochromaticity of the beam. It should be larger than the maximum path length difference in the sample; otherwise the loss of coherence would result in a reduction of the contrast at high wave vector transfer, where the path length difference is maximal. One can estimate the longitudinal coherence length at the XCS instrument as $\Lambda = \frac{1}{2} \times \frac{1.42 \times 10^{-10}}{1.4 \times 10^{-4}} \approx 0.5 \mu$m at 8.7 keV. A relation for the change in contrast as a function of longitudinal coherence length is given in Ref. 37. In the present context this is expressed by

$$\beta_r = \frac{2}{L^2 W^2} \int_0^L dx(L-x) \int_0^W dy(W-y)e^{-x^2/\xi^2}\left(e^{-|Ax+By|} + e^{-|Ax-By|}\right). \quad (5)$$

Here, L is the length of the sample transverse to the beam, $W = 1$ mm, is the width of the sample along the beam, $A = \frac{4\pi}{\Lambda}\frac{q}{k}\sqrt{1 - \frac{q^2}{4k^2}}$ and $B = \frac{2\pi}{\Lambda}\frac{q^2}{k^2}$. For the data presented in Fig. 3 and Fig. 4, the maximum wave vector transfer is $q = 0.041$Å^{-1}, and the value of L is given by the focal spot size, and thus varies from 3.3 to 4.7 microns. With 4.7 microns, both B and ξ can be neglected and the contrast is given by

$$\beta = \frac{2}{L^2} \int_0^L dx(L-x)e^{-Ax} = 2\frac{AL-1+e^{-AL}}{A^2L^2}. \quad (6)$$

This yields a theoretical minimum contrast of 0.84 for single pulse at the largest q value when the scattering is along the horizontal direction. Generally the deviation of the contrast from 1 is small and it slowly decays with q. Therefore, the longitudinal coherence length has only a limited effect on the contrast at wave vector transfers used in our experiment. It should be noted that the contrast observed during our experiment is about eight times lower than the theoretical value calculated above because we used multiple pulses exposure. This may most probably be attributed to the shot-to-shot spatial jitter of the XFEL focused beam.

Discussion
We have demonstrated that sequential XPCS on soft matter in its classical implementation is possible with an XFEL. We were able to deduce dynamics of a molten polymer by measuring the speckle pattern from the same sample position with a time between frames ranging from 7 s up to 1000 s with maximum total exposure of 0.8 ns (total 150 frames with 100 pulses per frame) at ~2.4×10^9 photons per pulse. Along with our estimate for the temperature increase in the sample, the sample damage does not constitute a limiting factor in the study of polymer dynamics using XFEL sources. However, the further examination of sample damage depending on the particle size and systematic study with different intensity levels, e.g., with and without an attenuator will be done in near future.

The shot-to-shot intensity and energy variations in the XFEL radiation, inherent to the SASE process, represent a challenge for data analysis since two consecutive frames may have a mean intensity varying by orders of magnitude. It can partially be compensated by proper normalization of the incoming intensity. These energy fluctuations should be much reduced by self-seeding[38] in the next generation of XFELs.

Since the X-ray beam entering the monochromator has a different energy spectrum for each shot, the number of temporal modes of the beam incident on the sample also fluctuates on a frame to frame basis. This implies a supplementary loss in contrast even for a fully spatially coherent beam if the path length difference is of the same order as the longitudinal coherence length[7].

In this study, we were able to reach up to a wave vector transfer q ~ 0.11Å^{-1} with a reasonable signal to noise ratio, i.e. slightly larger than the wave vector transfer achievable in the third generation synchrotrons. Although the brilliance of XFEL is orders of magnitude larger than for the third generation synchrotron sources, the number of photons per pulse is finally only of the order of 10^9 in monochromatic conditions. Therefore, one can deliver multiple pulses to the sample for each frame to increase the scattering intensity. Multiple pulse exposures can be a way of increasing the scattering intensity but it may be at the cost of a lower contrast, sample heating, and increasing the risk of damaging the sample, thus requiring beforehand a careful

examination of the experimental parameters. While the read-out time of the detector installed at that time at the XCS instrument prevented the study of shorter time scales than a few seconds, independent of the repetition rate, the split-and-delay unit[17–18] under commissioning will allow the study of relaxation times from nanoseconds to picoseconds by splitting a single shot. Moreover, faster 2D detectors, ideally with a reading out at 120 Hz to make full use of the repetition rate of the machine, and high-repetition rates FELs such as the European XFEL may allow the probing of dynamics from seconds to microseconds.

Methods

Sample preparation. The data presented in this study corresponds to gold nanoparticles (spheres of 5.5 nm diameter) grafted with polystyrene (M_w=30 kg/mol) in a polystyrene matrix (M_w=42 kg/mol). The nanoparticle size was chosen to match the radius of gyration of the polystyrene matrix, thus increasing the scattered intensity while still reflecting the polymer dynamics. Ligands (polystyrene) were first attached to gold nanoparticles in order to prevent agglomeration via the electrostatic interaction. Grafted nanoparticles were then mixed with the matrix polymer (polystyrene) to achieve a volume fraction of 0.5%. After the solution was completely mixed, the solvent was removed first and the solid sample was put in a transmission aluminum holder. The temperature for thermal annealing is 180°C for 24 hrs.

Experimental setup. The experiment was performed at the x-ray correlation spectroscopy (XCS) instrument at the Linac Coherent Light Source (LCLS) at SLAC National Accelerator Laboratory (Menlo Park, USA). The transverse coherence of the X-ray beam is built up through 32 undulators for a total length of ~105 m. The energy was set to 8.4 keV or 8.7 keV using a Si (111) double crystal monochromator with 1.4×10^{-4} bandwidth. The beam was focused using compound refractive lenses to achieve a beam size of 3.5 μm × 3.5 μm (H × V) at the sample position. The electron beam jitter and the random nature of the SASE process results in intensity fluctuations at the exit of the monochromator, thus normalization by the incident intensity on the sample is absolutely required before any further consideration.

Data were collected at a sample to detector distance of 5037 mm or 685 mm with a Princeton Instruments LCX-1300 CCD camera, composed of an array of 1340 × 1300 pixels with a pixel size of 20 μm². The CCD was set either on the diffractometer detector arm, to achieve a sample to detector distance (SDD) less than 1 m, or on the large angle detector mover (SDD from 4 m to 8 m). Both configurations allow reaching high wave vector transfers by changing the detector angle. Various combinations of pulses per frame (1, 2, 5, 10, 20, 30, 50, 100, 200 or 400 pulses per frame) were used. These consecutive pulses were sent at a rate of 120 Hz. However, the read-out time of the detector was Δt_{min}=7 s, thus presenting a strong limitation on the minimum accessible delay time between frames which is far from 120 Hz LCLS repetition rate.

The average number of photons at the exit of the undulator was 9.2×10^{11} photons per pulse. The transmission coefficients at each optical component in the beamline at 8.7 keV are summarized in the Supplementary Table 3. The total transmission is 2.565×10^{-3} and the average number of incident photons on the sample is about 2.4×10^{9} per pulse.

Data analysis. Data analysis was carried out after dark subtraction and normalization by the intensity incident on the sample. The monitor chosen for the normalization was located after the monochromator and compound refractive lenses. g_2 functions were calculated via a multi-tau algorithm with symmetric normalization scheme[39–40], which allows significant reductions of noise levels at large delay times. The analysis was cross-checked with single tau sequential analysis.

1. Redecke, L. *et al.* Natively Inhibited *Trypanosoma brucei* Cathepsin B Structure Determined by Using an X-ray Laser. *Science* **339**, 227–230 (2012).
2. Glover, T. E. *et al.* X-ray and optical wave mixing. *Nature* **488**, 603–608 (2012).
3. Clark, J. N. *et al.* Ultrafast Three-Dimensional Imaging of Lattice Dynamics in Individual Gold Nanocrystals. *Science* **341**, 56–59 (2013).
4. Grübel, G., Stephenson, G. B., Gutt, C., Sinn, H. & Tschentscher, T. XPCS at the European X-Ray free electron laser facility. *Nucl. Instrum. Methods Phys. Res. B* **262**, 357–367 (2007).
5. Saldin, E. L., Schneidmiller, E. A. & Yurkov, M. V. Statistical properties of radiation from VUV and X-ray free electron laser. *Opt. Commun.* **148**, 383–403 (1998).
6. Lee, S. *et al.* High wavevector temporal speckle correlations at the Linac Coherent Light Source. *Opt. Express* **20**, 9790–9800 (2012).
7. Gutt, C. *et al.* Single shot Spatial and Temporal Coherence Properties of the SLAC Linac Coherent Light Source in the Hard X-Ray Regime. *Phys. Rev. Lett.* **108**, 024801 (2012).
8. Gutt, C. *et al.* Measuring temporal speckle correlations at ultrafast x-ray sources. *Opt. Express* **17**, 55–61 (2009).
9. Goodman, J. *Speckle Phenomena in Optics: Theory and Application.* (Roberts & Company Publishers, Greenwood Village, 2007).
10. Hruszkewycz, S. O. *et al.* High Contrast X-ray Speckle from Atomic-Scale order in Liquids and Glasses. *Phys. Rev. Lett.* **109**, 185502 (2012).
11. Livet, F. *et al.* Kinetic evolution of unmixing in an AlLi alloy using x-ray intensity fluctuation spectroscopy. *Phys. Rev. E* **63**, 036108 (2001).
12. Shpyrko, O. G. *et al.* Direct measurement of antiferromagnetic domain fluctuations. *Nature* **447**, 68–71 (2007).
13. Kim, H. *et al.* Surface Dynamics of Polymer Films. *Phys. Rev. Lett.* **90**, 068302 (2003).
14. Jiang, Z. *et al.* Evidence for Viscoelastic Effects in Surface Capillary Waves of Molten Polymer Films. *Phys. Rev. Lett.* **98**, 227801 (2007).
15. Jiang, Z. *et al.* Entanglement Effects in Capillary Waves on Liquid Polymer Films. *Phys. Rev. Lett.* **101**, 246104 (2008).
16. Stephenson, G. B. *et al.* LCLS: The First Experiments. *www-ssrl.slac.stanford.edu/lcls/papers/lcls_experiments_2.pdf* (2000), date of access: 19/07/2014.
17. Roseker, W. *et al.* Performance of a picosecond x-ray delay line unit at 8.39 keV. *Optics Letters* **34**, 1768–1770 (2009).
18. Roseker, W. *et al.* Development of a hard X-ray delay line for X-ray photon correlation spectroscopy and jitter-free pump-probe experiments at X-ray free-electron laser sources. *J. Synchrotron Rad.* **18**, 481–491 (2011).
19. Dixon, P. K. & Durian, D. J. Speckle Visibility Spectroscopy and Variable Granular Fluidization. *Phys. Rev. Lett.* **90**, 184302 (2003).
20. Bandyopadhyay, R., Gittings, A. S., Suh, S. S., Dixon, P. K. & Durian, D. J. Speckle-visibility spectroscopy: A tool to study time-varying dynamics. *Rev. Sci. Instrum.* **76**, 093110 (2005).
21. DeCaro, C. *et al.* X-Ray speckle visibility spectroscopy in the single-photon limit. *J. Synchrotron Rad.* **20**, 332–338 (2012).
22. Robert, A. *et al.* The X-ray Correlation Spectroscopy instrument at the Linac Coherent Light Source. *J. Phys.: Conf. Ser.* **425**, 212009 (2013).
23. Robert, A., Wandersman, E., Dubois, E., Dupuis, V. & Perzynski, R. Glassy dynamics and aging in a dense ferrofluid. *Europhy. Lett.* **75**, 764–770 (2006).
24. Cipelletti, L. & Ramos, L. Slow dynamics in glassy soft matter. *J. Phys.: Condens. Matter* **17**, R253–R285 (2005).
25. Narayanan, S., Lee, D. R., Hagman, A., Li, X. & Wang, J. Particle Dynamics in Polymer-Metal Nanocomposite Thin Films on Nanometer-Length Scales. *Phys. Rev. Lett.* **98**, 185506 (2007).
26. Brown, G., Rikvold, P. A., Sutton, M. & Grant, M. Speckle from phase-ordering systems. *Phys. Rev. E* **56**, 6601–6612 (1997).
27. Malik, A. *et al.* Coherent X-Ray Study of Fluctuations during Domain Coarsening. *Phys. Rev. Lett.* **81**, 5832–5835 (1998).
28. Solomon, M. J. & Varadan, P. Dynamic structure of thermoreversible colloidal gels of adhesive spheres. *Phys. Rev. E* **63**, 051402 (2001).
29. Bearden, J. A. & Burr, A. F. Reevaluation of X-Ray Atomic Energy Levels. *Rev. Mod. Phys.* **39**, 125–142 (1967).
30. Yeh, J. J. & Lindau, I. Atomic subshell photoionization cross sections and asymmetry parameters: 1 ≤ Z ≤ 103. *At. Data Nucl. Data Tab.* **32**, 1–155 (1985).
31. Powell, C. J. & Jablonski, A. Evaluation of Calculated and Measured Electron Inelastic Mean Free Paths Near Solid Surfaces. *J. Phys. Chem. Ref. Data* **28**, 19–62 (1999).
32. Bearden, J. A. X-Ray Wavelengths. *Rev. Mod. Phys.* **39**, 78–142 (1967).
33. Childs, K. D. *et al.* Handbook of Auger Electron Spectroscopy. [Hedberg, C. L. (ed)] (Physical Electronics, Eden Prairie, 1995).
34. Hubbell *et al.* A Review, Bibliography, and Tabulation of K, L, and Higher Atomic Shell X-Ray Fluorescence Yields. *J. Phys. Chem. Ref. Data* **23**, 339–364 (1994).
35. Pu, Z. *Polymer Data Handbook.* [Mark, J. E. (ed)](Oxford University Press, New York, 1999).
36. Plazek, D. J. & O'Rourke, V. M. Viscoelastic Behavior of Low Molecular Weight Polystyrene. *J. Polym. Sci.* Part A-2 **9**, 209–243 (1971).
37. Sandy, A. R., Lurio *et al* Design and characterization of an undulator beamline optimized for small-angle coherent X-ray scattering at the Advanced Photon Source. *J. Synchrotron Rad.* **6**, 1174–1184 (1999).
38. Amann, J. *et al.* Demonstration of self-seeding in a hard-X-ray free-electron laser. *Nature Photon.* **6**, 693–698 (2012).
39. Schätzel, K. Noise on photon correlation data: I. Autocorrelation functions. *Quantum Opt.* **2**, 287–305 (1990).
40. Sikorski, M., Jiang, Z., Sprung, M., Narayanan, S., Sandy, A. R. & Tieman, B. A graphical user interface for real-time analysis of XPCS using HPC. *Nucl. Instrum. Meth Phys. Res. A* **649**, 234–236 (2011).

Acknowledgments

Author contributions

H.K., A.R., G.G. and S.K.S. designed research. J.C., W.C., J.K., Z.J., H.C.L., C.J.Y., S.N. prepared the experimental setup. M.C., I.K., T.E., T.P.R. synthesized and prepared the samples. J.C., W.C., J.W., J.K., Z.J., S.S., M.S., S.-W.C., Y.D., Y.M., H.G., C.G., L.B.L., O.S., A.R., S.K.S., H.K. carried out the experiment. J.C., J.W. and Z.J. analyzed and modeled the data. J.C. and H.K. wrote the manuscript text. All authors reviewed and discussed the manuscript.

Additional information